Supplementary Information (SI) for Nanoscale.
This journal is © The Royal Society of Chemistry 2024

Supplementary Information

Ultralight Flexible 3D Nickel Micromesh Decorated with NiCoP for High Stability Alkaline Zinc Batteries

Zana Karim Abdul[1,3], Zeqi Nie[1], Yapeng Zhang[1], XiuXue Liu[1], XiaohuWang[1], Niwamanya Gilbert[1], Donghai Wei[1,2], Wen Zhang[4]*, Guanhua Zhang[1,3]*

[1] State Key Laboratory of Advanced Design and Manufacturing Technology for Vehicle, College of Mechanical and Vehicle Engineering, Hunan University, Changsha 410082, China

[2] Hunan University of Technology, Zhuzhou 412008, China

[3] Greater Bay Area Institute for Innovation, Hunan University, Guangzhou 511300, China

[4] Department of Chemical and Materials Engineering, the University of Auckland, Auckland CBD, Auckland 1142, New Zealand

E-mail: weidonghai000@126.com; zhang.wen@auckland.ac.nz

Table of Contents

Chemical reagents P4

Experimental methods P5

Material characterization and electrochemical measurements.....P6

Figure S1. Thickness measurements of a) 3D NM and b) zinc foil.....P7

Figure S2. Digital photograph of Ni mesh showing a) Lightness and flexibility of the Ni mesh, and b) transparency of the Ni mesh.....P8

Figure S3. Elemental mapping images of the 3D NM@NiCoP.....P9

Figure S4. The sheet resistance of a) NM mesh, and b) 3D NM electrode.....P10

Figure S5. a) XRD patterns of Ni, 3D NM and 3D NM@NiCoP, b) Raman spectrum of 3D NM@NiCoP. P11

Figure S6. a) Rate performance, (b) capacity comparison and.....P12

Figure S7. Schematic illustration of the fabrication process for Zn@TiO_2. a) Zinc foil, b) Zinc foil after coating with a 20 nm TiO_2 layer.....P13

Figure S8. Digital photograph of the zinc plate before (left) and after (right) coating with 20 nm TiO_2 via ALD.....P14

Figure S9. Digital photographs of the surface layer of Zn@TiO_2 anodes after immersion in KOH with (a-c) cleaned and (b-d) Non-cleaned Zn foil.....P15

Figure S10. Electrochemical performance of Zn@TiO_2//3D NM@NiCoP in 2 M KOH.....P16

Figure S11. Two-electrode corrosion test of Zn@TiO_2//3D NM@NiCoP.....P17

Figure S12. Schematic illustration of the fabrication process for 3D Zn@Al_2O_3@TiO_2.....P18

Figure S13. Comparative I-V tests for Zn foil, Zn@ TiO_2 and Zn@Al_2O_3@TiO_2.....P19

Figure S14. Contact angles of a) bare Zn b) Zn@TiO_2 and c) Zn@Al_2O_3@TiO_2 with water droplets.....P20

Figure S15. Surface XRD patterns of Zn foil, Zn@TiO_2 and Zn@Al_2O_3@TiO_2 electrodes.....**P21**

Figure S16. a) Comparison of the areal capacity of theZn@Al_2O_3@TiO_2//3D NM@NiCoP with results from other studies at various current densities, b) comparison of cycling stability between devices with Zn@TiO_2 and Zn@AL_2O_3@TiO_2 anodes at same current density of 3 mA cm^{-2} in a two-electrode system.....**P22**

Table S1. Performance comparison of relevant works in a three-electrode system.....**P23**

Table S2. Performance comparison of energy storage devices in a 2-Electrode Cell.....**P24**

Table S3. Comparison of the cycling stability of Zn@Al_2O_3@TiO_2//3D NM@NiCoP from this work with other materials used in electrochemical energy storage devices in units of cm^2.....**P25**

Supplementary references.....**P26**

Chemical Reagents

Nickel sulfate hexahydrate ($NiSO_4 \cdot 6H_2O$, AR, Aladdin), nickel chloride hexahydrate ($NiCl_2 \cdot 6H_2O$, ≥ 98.0%, Aladdin), ammonium chloride (NH_4Cl, 99.5%, Aladdin), $CoSO_4 \cdot 7H_2O$ (≥ 99.0%, Aladdin), $NaH_2PO_4 \cdot H_2O$ (AR, Aladdin), $C_6H_5Na_3O_7 \cdot 2H_2O$ (AR, Aladdin), sodium hydroxide (NaOH, AR, Aladdin), potassium hydroxide (KOH, ≥ 85%, Aladdin), lithium hydroxide monohydrate ($LiOH \cdot H_2O$, 98%, Aladdin), boric acid (H_3BO_3, ≥ 99.5%, Aladdin), sulfuric acid (H_2SO_4, ACS reagent, 95.0-98.0 %), all the chemicals were of analytical grade and used without further purification.

Indium tin oxide (ITO) was purchased from South China Xiang Cheng Technology Co., Ltd. The photoresist (PR, RZJ-390PG-50CP) was obtained from Suzhou Rui Hong Electronic Chemical Co., Ltd. Deionized water used in all experiments was prepared using a Hitech-K flow water purification system (Hitech Instrument Co., Ltd., Shanghai, China).

Experimental methods

Fabrication of 3D Ni Mesh (NM)

A layer of photoresist was first spin-coated onto the indium tin oxide (ITO) substrate at sequential spin speeds of 500 rpm for 10 s and 800 rpm for 30 s. The ITO substrates were then dried at 100°C for 3 minutes. Using a 3D honeycomb-patterned mask plate (7.5 μm, 100 × 100 mm) and exposed to a specific UV wavelength, the photoresist underwent a photochemical reaction, resulting in areas with different solubility. Unexposed photoresist was removing using 0.5% NaOH, yielding precise lithographic patterns. To create an ordered cellular array network, micro-gullies were filled by selective electrodeposition of Ni foam at 2 V and 30 mA cm^{-2} for 2400 s. The bath solution composed 7.85 mg $NiSO_4 \bullet 6H_2O$ and 1.3 mg NH_4Cl. The Ni micromesh (NM) was then peeled off from the ITO by immersing in an etching solution containing 5% NaOH for 1 minute. The resulting 3D Ni mesh had a thickness of approximately 0.004 mm, as shown in Figure S1a.

Preparation of 3D NM@NiCoP electrode

In the secondary electrodeposition process, a self-supporting 3D NM (1×1cm^2) was immersed in a solution containing 20 mg $NiCl_2 \cdot \bullet 6H_2O$, 4 mg NH_4Cl and 10 mg H_3BO_3 in 100 ml of deionized water (DI). The bath temperature was maintained at 60 °C, and a current density of 10 mA cm^{-2} was applied for 600 seconds. NiCoP was electrodeposited onto the 3D Ni mesh to obtain 3D NM@NiCoP. The electrochemical deposition was performed in a standard three-electrode cell (CH1660E), with the 3D Ni mesh as the working electrode, platinum as the counter electrode, and Hg/HgO as the reference electrode. Cycling voltammetry (CV) was conducted with the potential range from -0.3V to -1.2 V at a scan rate of 2 mV s^{-1} for 60 cycles. The solution comprised 0.3 mg $NiSO_4 \bullet 6H_2O$, 0.3514 mg $CoSO_4 \bullet 7H_2O$, 2.6 mg $NaH_2PO_4 \bullet H_2O$ and 1.47 mg $C_6H_5Na_3O_7 \bullet 2H_2O$ in 50 ml ID water.

Preparation of $Zn@Al_2O_3@TiO_2$ anode

Zinc foil (Zn, 99.9%, 5×5cm) was ultrasonically cleaned in ethanol and DI water to remove surface impurities and then dried at 60°C in vacuum oven for 45 minutes. Using the NCE-200 R atomic layer deposition system, a 10 nm layer of Al_2O_3 was coated onto the prepared Zn plate at 130°C, followed by the deposition of a 20 nm layer of TiO_2 at 120°C on the $Zn@Al_2O_3$.

Material characterization and Electrochemical Measurements

Microstructure analysis of the samples was conducted using field-emission scanning electron microscopy (SEM) (Carl Zeiss SIGMA HD) and optical microscopy (Carl-Zeiss AXIO-10). Raman spectra were obtained using a confocal microscopy system with a 532 nm laser wavelength (WITec Alpha-300 R) at room temperature. X-ray diffraction (XRD) patterns were acquired using an Siemens D-5000 diffractometer. Electrochemical depositions were carried out using an electrochemical workstation (CHI660e) and a source meter. All electrochemical measurements, including cyclic voltammetry (CV), galvanostatic charge-discharge (GCD) and electrochemical impedance spectroscopy (EIS), were conducted in a 2 M KOH solution at room temperature using the same electrochemical workstation. In these experiments, the synthesized samples served as the working electrode, while a Pt sheet, and a mercuric oxide electrode (HgO) were used as the counter electrode and the reference electrode, respectively. The charge storage properties of the asymmetric device, constructed with the $Zn@AL_2O_3@TiO_2$ anode and the 3D NM@NiCoP cathode, were evaluated under a two-electrode mode using the electrochemical station.
The areal capacity was calculated according to the following equation:

$$C_a = I \times \Delta t \div (S \times 3.6) \qquad (1)$$

Where C_a (μAh cm^{-2}) represents the areal capacitance, I (mA) is the charge/discharge current, Δt (s) is the discharge time, and S is the loading area of the active material (1 × 1 cm^2 in this work).

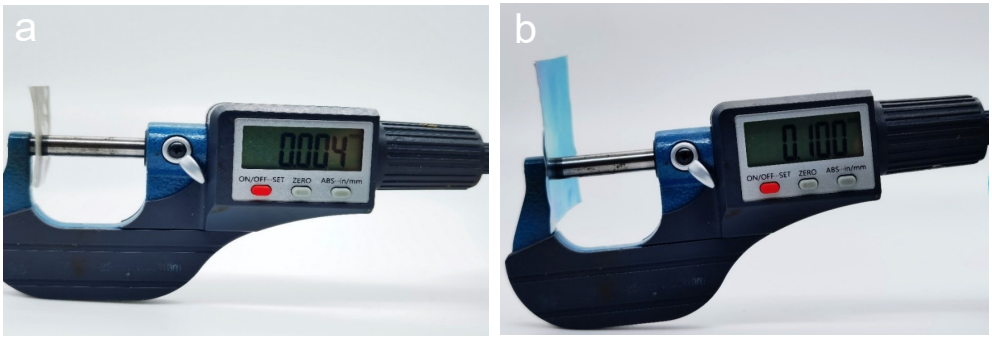

Figure S1. Thickness measurements of a) 3D NM: 0.004 mm and b) zinc foil: 0.1 mm.

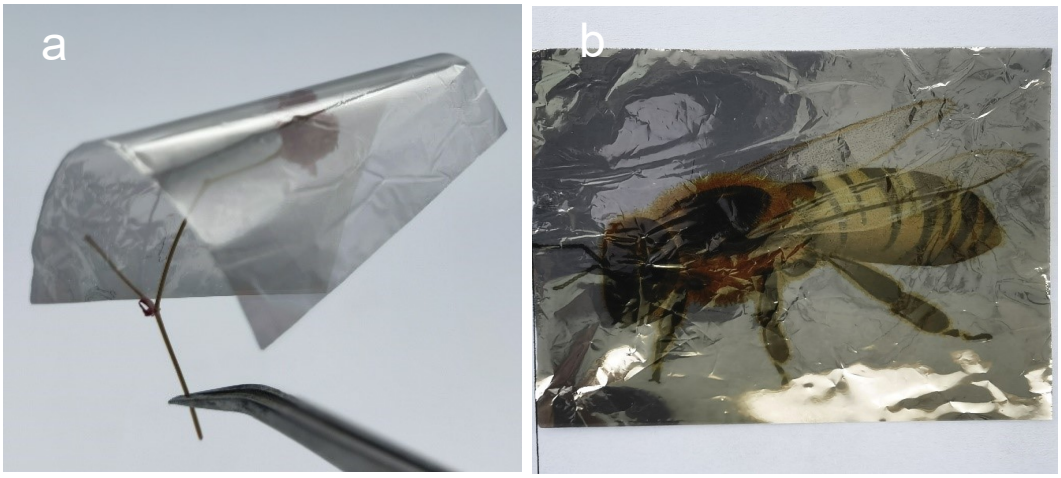

Figure S2. Digital photograph of Ni mesh showing a) lightness and flexibility of the Ni mesh, and b) transparency of the Ni mesh.

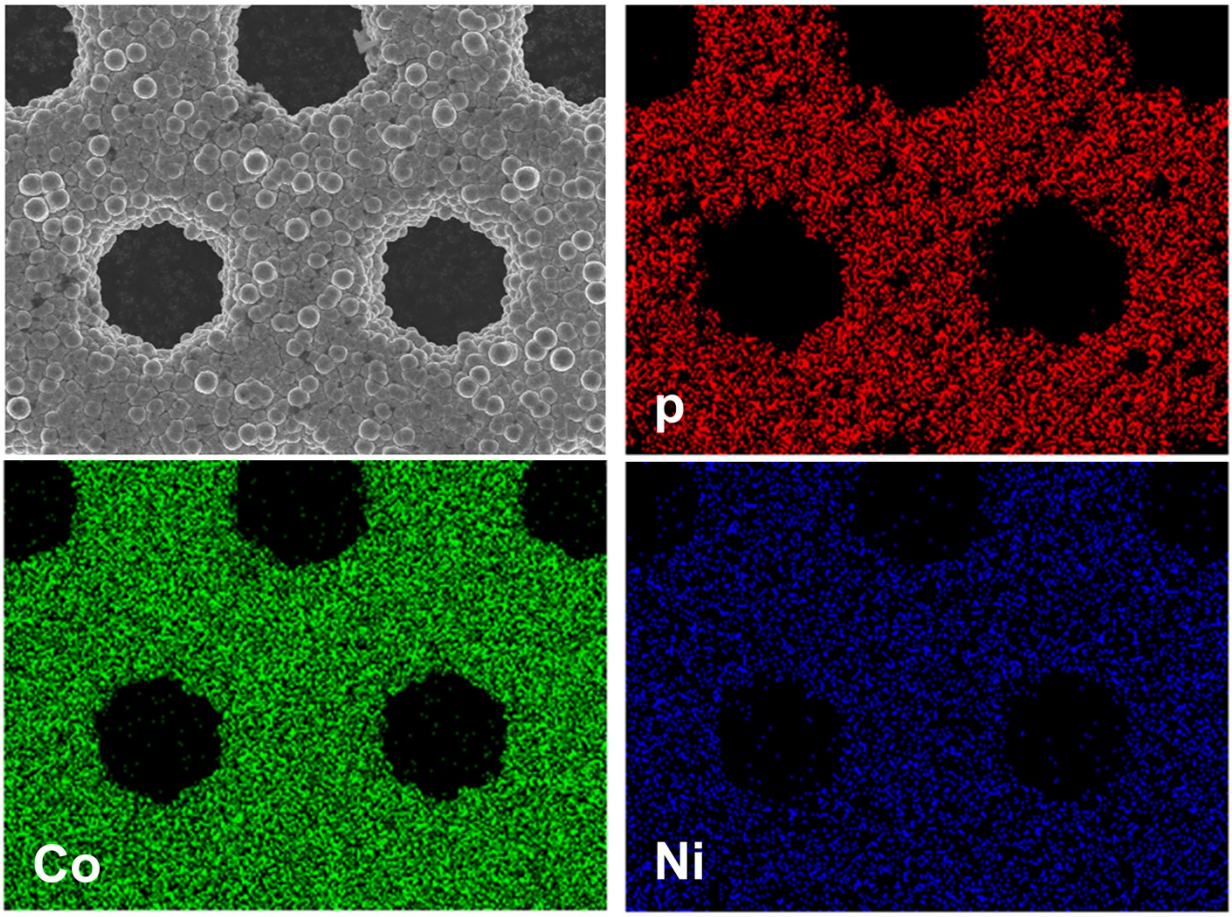

Figure S3. SEM image and the corresponding elemental mapping images of the 3D NM@NiCoP.

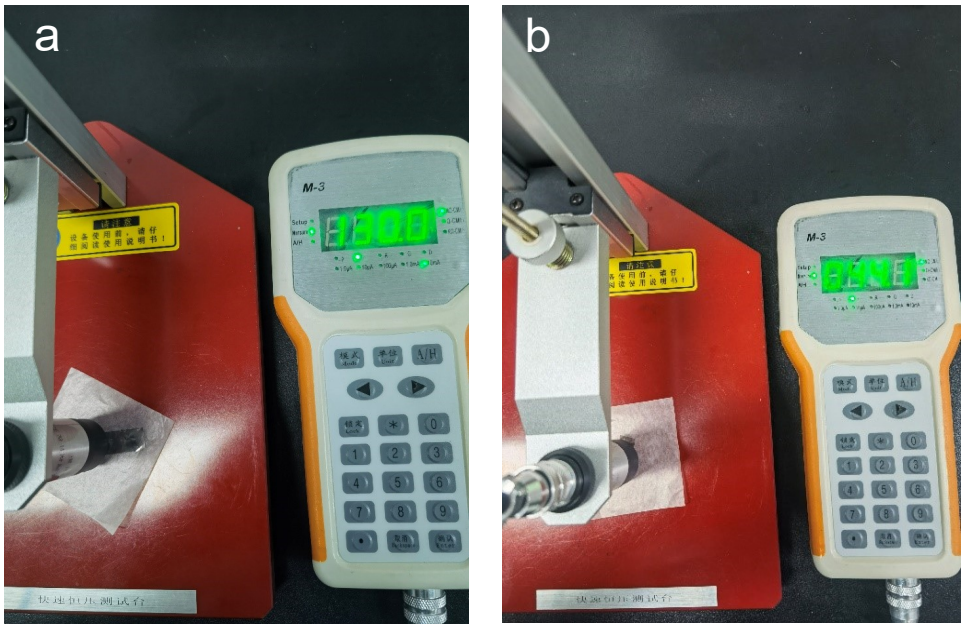

Figure S4. The sheet resistance of a) NM electrode and b) 3D NM electrode.

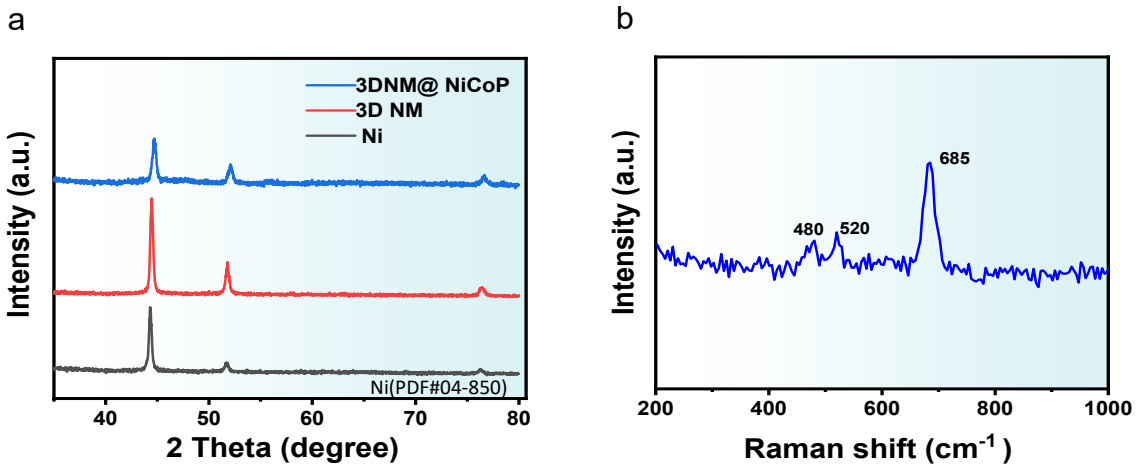

Figure S5. a) XRD patterns of Ni, 3D NM and 3D NM@NiCoP, b) Raman spectrum of 3D NM@NiCoP.

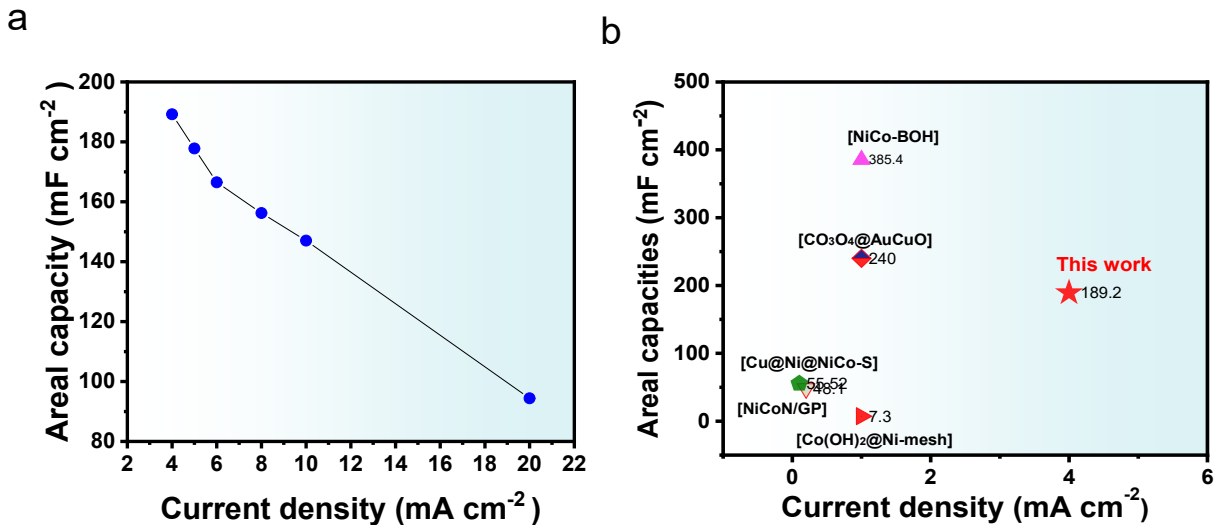

Figure S6. a) Rate performance of 3D NM@NiCoP, b) comparison of the rate capabilities in this work with reported NiCoP values (transformed from literature data).[2, 3, 5, 6, 11]

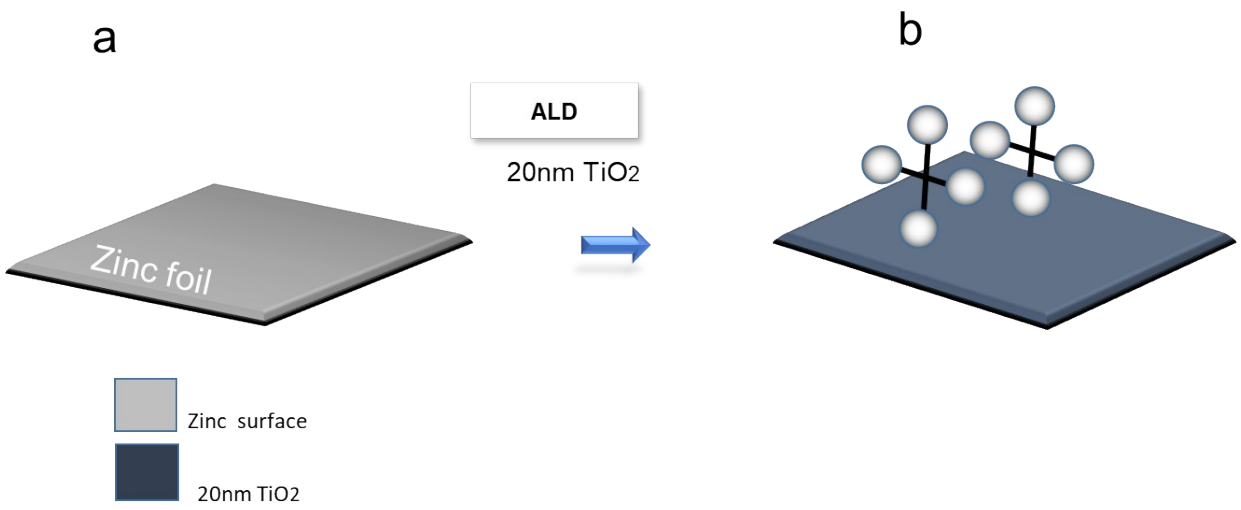

Figure S7. Schematic illustration of the fabrication process for Zn@TiO_2. a) zinc foil, b) zinc foil after coating with a 20 nm TiO_2 layer.

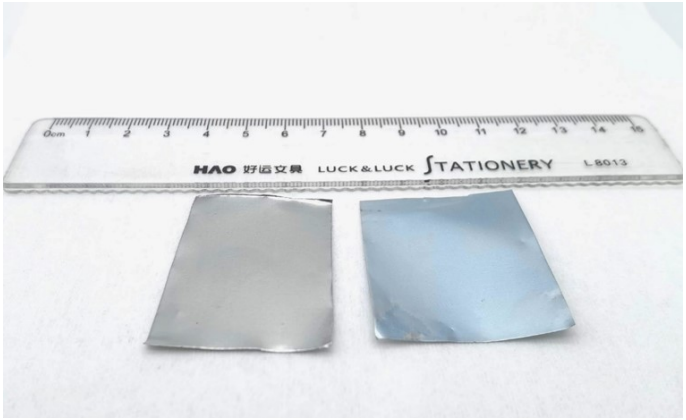

Figure S8. Digital photograph of the zinc plate before (left) and after (right) coating with 20 nm TiO_2 via ALD.

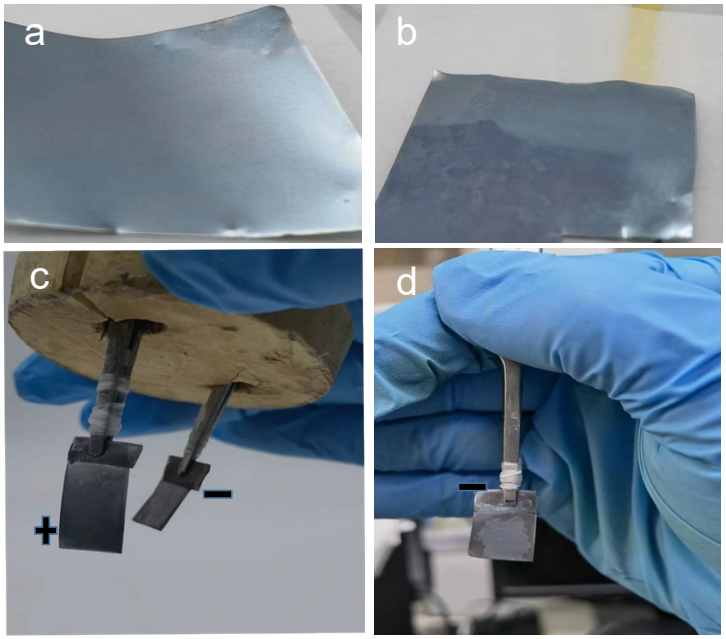

Figure S9. Digital photographs showing the surface of Zn@TiO_2 anodes after immersion in KOH: a-c) cleaned Zn foil coated with TiO_2, with the surface remaining intact and stable after more than 28 hours in KOH, b-d) Non-cleaned Zinc foil coated with TiO_2, where the ALD layer is compromised after more than 28 hours in KOH.

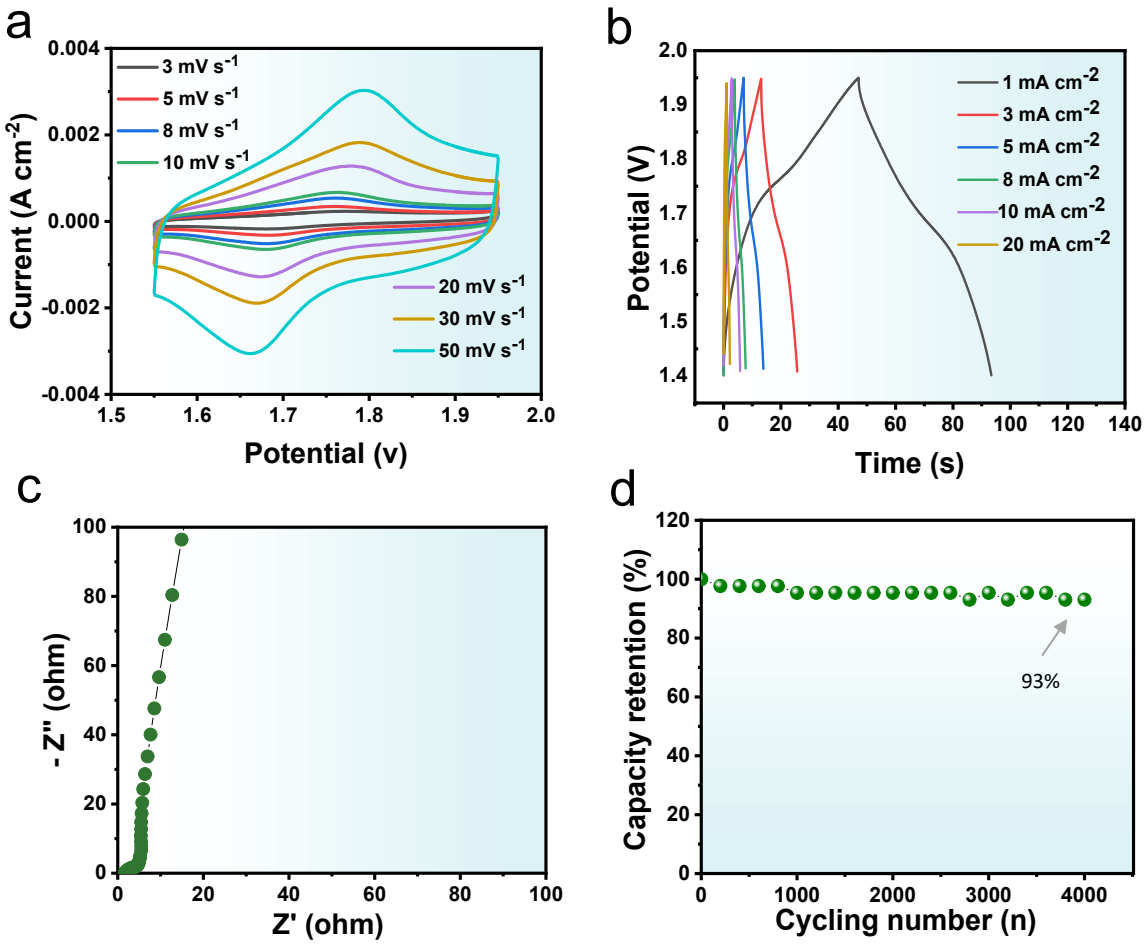

Figure S10. Electrochemical performance of Zn@TiO_2//3D NM@NiCoP in 2 M KOH: a) Cyclic voltammetry (CV) curves, b) galvanostatic charge-discharge (GCD) curves, c) Nyquist impedance spectra (EIS), d) plot of maximum capacity at a current density of 3 mA cm^{-2}.

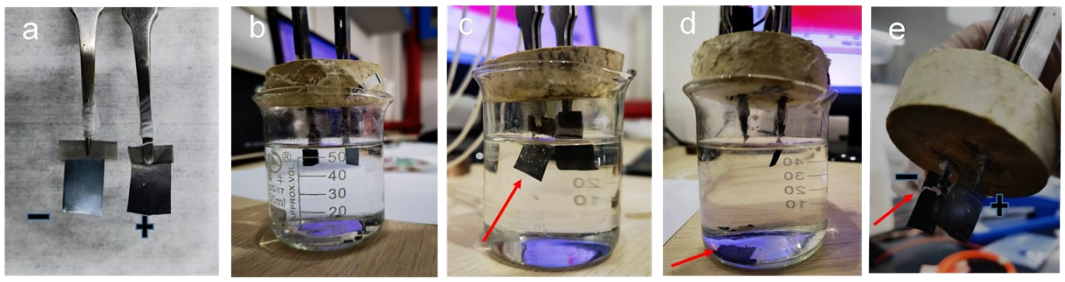

Figure S11. Two-electrode corrosion test for Zn@TiO_2//3D NM@NiCoP: a) anode and cathode appearances, b) anode and cathode in 2M KOH, c) Zn@TiO_2 in 2 M KOH showing significant hydrogen evolution, d) Zn@TiO_2 varnished in the solution and e) corrosion of Zn@TiO_2.

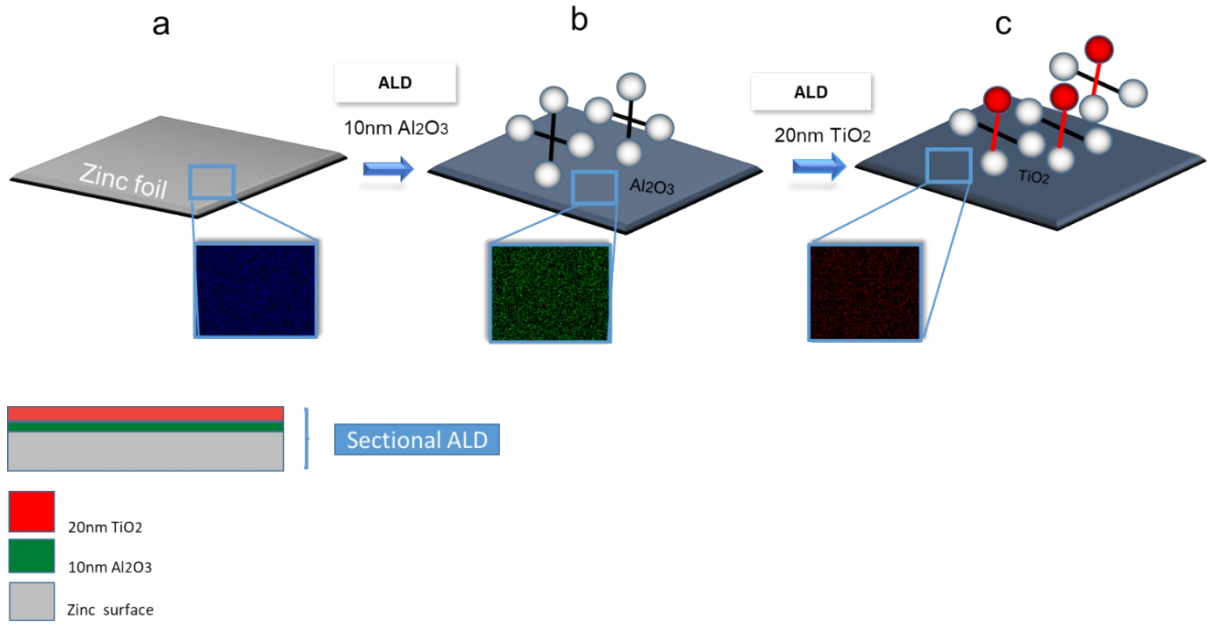

Figure S12. Schematic illustration of the fabrication process for 3D $Zn@Al_2O_3@TiO_2$ with different coatings architectures: a) zinc foil, b) coated with 10 nm Al_2O_3 c) $Zn@Al_2O_3$ after additional 20 nm TiO_2 coating.

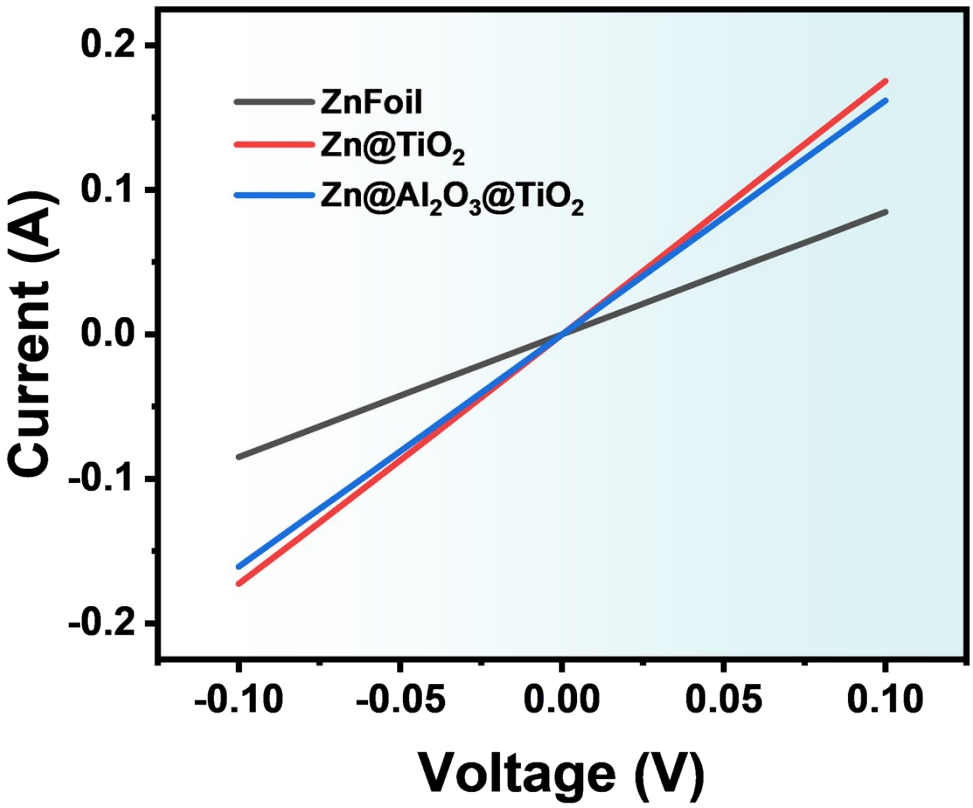

Figure S13. Comparative I-V tests for Zn foil, Zn@ TiO_2 and Zn@Al_2O_3@TiO_2.

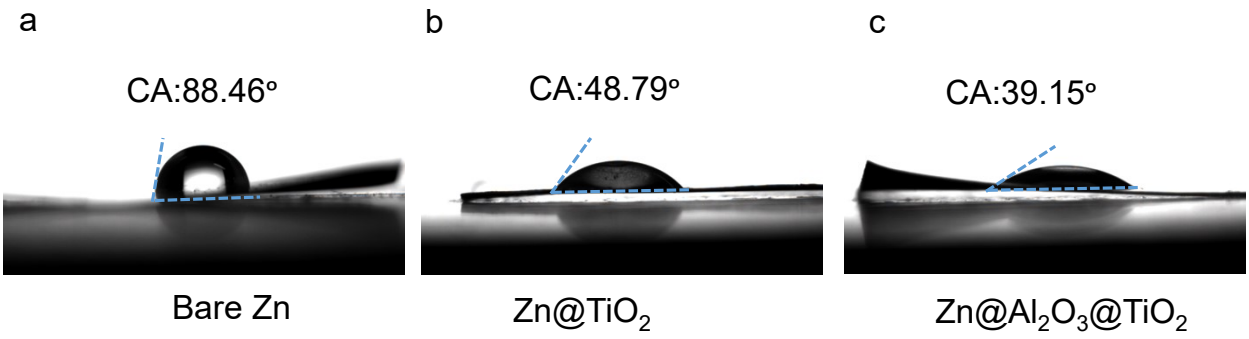

Figure S14. Contact angles of a) bare Zn b) $Zn@TiO_2$ and c) $Zn@Al_2O_3@TiO_2$ with water droplets.

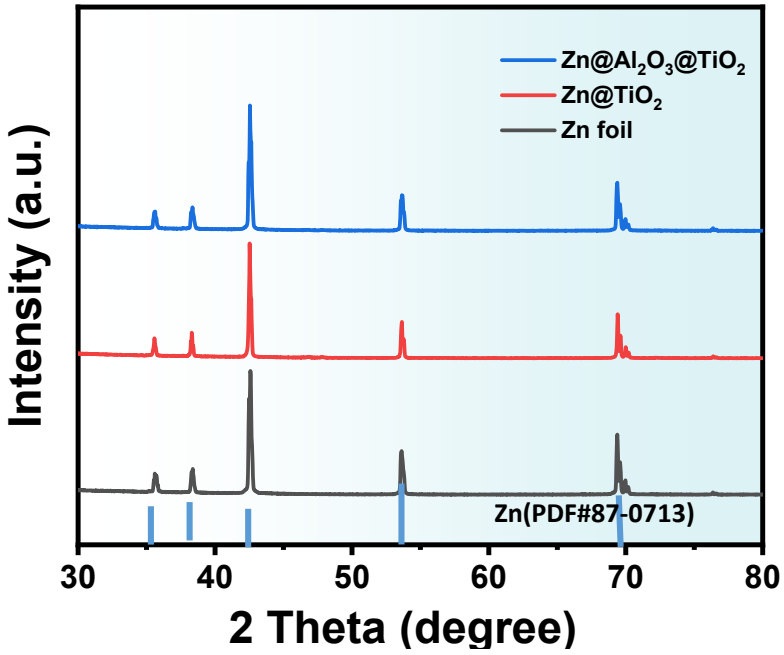

Figure S15. Surface XRD patterns of Zn foil, Zn@TiO_2 and Zn@Al_2O_3@TiO_2 electrodes.

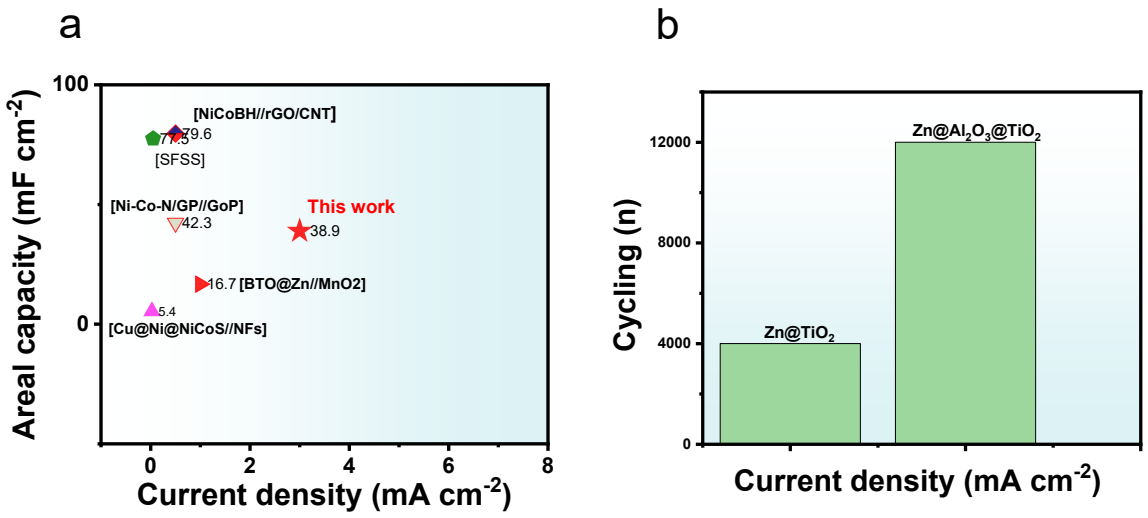

Figure S16. a) Comparison of the areal capacity of the$Zn@Al_2O_3@TiO_2$//3D NM@NiCoP with results from other studies at various current densities, b) comparison of cycling stability between devices with $Zn@TiO_2$ and $Zn@AL_2O_3@TiO_2$ anodes at same current density of 3 mA cm^{-2} in a two-electrode system.

Table S1 Performance comparison of relevant works in a three-electrode system.

Electrode Materials	Current Density	Capacitance	Working Electrode	Electrolyte	Ref.
3D NM@NiCoP	4 mA cm^{-2}	26.1 μAh cm^{-2}	1×1 cm^2	2M KOH	This work
3D NM@NiCo BH	1 mA cm^{-2}	75.58 μAh cm^{-2}	1×1 cm^2	2M KOH	[1]
NM@NiCoBH	1 mA cm^{-2}	12 μAh cm^{-2}	1×1cm^2	1M KOH	[2]
NM@NiCoP	1 mA cm^{-2}	11 μAh cm^{-2}	1×1cm^2	2M KOH	[3]
3D CoNiDHs/$NiCo_2O_4$/CFP	10 mA cm^{-2}	67 μAh cm^{-2}	3×4 cm^2	1M KOH	[4]
Ni-CoN/GP	0.2 mA cm^{-2}	6.7 μAh cm^{-2}	1.5×2 cm^2	3M KOH	[5]
CO_3O_4@Au@CuO	1 mA cm^{-2}	33.3 μAh cm^{-2}	/	1M Na_2SO_4	[6]
NiCo-BOH	1 mA cm^{-2}	42.2 μAh cm^{-2}	/	1M KOH	[7]
L-MCH	3 mA cm^{-2}	49 μAh cm^{-2}	1×2 cm^{-2}	4M KOH	[8]
Ni/Co-N-350	2 mA cm^{-2}	53 μAh cm^{-2}	/	1M KOH	[9]
MoS_2@Ni mesh	1 mA cm^{-2}	1.62 μAh cm^{-2}	1×2 cm^{-2}	1M Na_2SO_4	[10]
Cu@Ni@Ni:Co-S	0.066 mAcm^{-2}	6.94 μAh cm^{-2}	1×2 cm^2	PVA-KOH	[11]
Co_3O_4@NiO	5 mA cm^{-2}	2.91 mAh cm^{-2}	1×1 cm^2	6M KOH	[12]
CC-CF@NiO	5 mA cm^{-2}	0.35 mAh cm^{-2}	2×2 cm^2	2M KOH	[13]

Table S2. Performance comparison of energy storage devices in a 2-electrode system.

Anode	Cathode	Electrolytes	Capacity	Current Density	Ref
$Zn@Al_2O_3@TiO_2$	3D NM@NiCoP	2 M KOH	5.42 μAh cm^{-2}	3 mA cm^{-2}	This work
RGO HSC	NiCo-P/Pox	6 M KOH	67.4 μAh cm^{-2}	2 mA cm^{-2}	[14]
Zn	$NiCO_2O_4$	1 M KOH	57.3 μAh cm^{-2}	0.5 mA cm^{-2}	[15]
GOP	Ni-Co-N/GP	PVA-KOH	18.8 μAh cm^{-2}	0.5 mA cm^{-2}	[5]
rGO/CNT	NiCoBH	PVA-KOH	29.18 μAh cm^{-2}	0.5 mA cm^{-2}	[7]
Cu@Ni@Ni:Co-S NFs	Cu@Ni@Ni:Co-S NFs	PVA-KOH	1.21 μAh cm^{-2}	0.025 mA cm^{-2}	[11]
C-pen ink	Ni-pen ink	1 M Na_2SO_4	4.64 μAh cm^{-2}	1 mA cm^{-2}	[16]
PEDOT-S:PSS	PEDOT-S:PSS	1 M H_3PO_4	23.5 μAh cm^{-2}	1 mA cm^{-2}	[17]
siloxene nanosheets	Zn	WiS	3.11 μAh cm^{-2}	0.05 mA cm^{-2}	[18]
Ag NW/graphene	AgNW@NiCo/NiCo$(OH)_2$	2 M KOH	3.2 μAh cm^{-2}	0.2 mA cm^{-2}	[19]
MnO NP/TC/ITO NP/TC)50	MnO NP/TC/ITO NP/TC)50	PVA/LiCl	2.24 μAh cm^{-2}	0.05 mA cm^{-2}	[20]

Table S3. Comparison of the cycling stability of $Zn@Al_2O_3@TiO_2$//3D NM@NiCoP from this work with other materials used in electrochemical energy storage devices in units of cm^2.

cathode	anode	electrolyte	Potential/V	capacitance	cycling	Ref
3D NM@NiCoP	$Zn@Al_2O_3@TiO_2$	KOH	1.4-1.95	5.42 μAh cm^{-2} (3 mA cm^{-2})	91% 11000 cycles	This work
CNT	Zn	$ZnSO_4$	0.2−1.8	34.67 μAh cm^{-2} (1 mA cm^{-2})	87.4% 6000 cycles	21
poly(4,40-TDP)/AC	Zn	$ZnSO_4$	0.1−1.9	1.2 mAh cm^{-2} (1 mA cm^{-2})	71% 2000 cycles	22
Ti_3C_2 MXene	Zn/CNT	$ZnSO_4$	0.1-1.2	81.5 μAh cm^{-2} (10 mA cm^{-2})	86.5% 6000 cycles	23
$Ti3C_2Tx$	Zn	PVA/$ZnCl_2$	0-1.4	43.6 μAh cm^{-2} (10 mV s^{-1})	54.7% 50000 cycles	24
MnO_2	$100Al_2O_3$@Zn	$Zn(SO_3CF_3)_2$	0.8-1.8	3.96 μAh cm^{-2} (1 mA cm^{-2})	89.4% 1000 cycles	25
MnO NP/TC/ITO NP/TC)50	MnO NP/TC/ITO NP/TC)50	PVA/LiCl	0-0.8	0.76 μAh cm^{-2} (0.5 mA cm^{-2})	76% 5000 cycles	20
Ni-Co-N/GP	GOP	PVA-KOH	0-1.5	12.9 μAh cm^{-2} (5 mA cm^{-2})	89% 8000 cycles	5
Cu@Ni@Ni:Co-S NFs	Cu@Ni@Ni:Co-S NFs	PVA-KOH	0-0.8	0.45 μAh cm^{-2} (0.075 mA cm^{-2})	92% 10000 cycles	11

References

1. G. Zhang, J. Hu, Y. Nie, Y. Zhao, L. Wang, Y. Li, H. Liu, L. Tang, X. Zhang, D. Li, L. Sun and H. Duan, *Advanced Functional Materials*, 2021, **31**, 2100290.
2. T. Chen, Z. Shuang, J. Hu, Y. Zhao, D. Wei, J. Ye, G. Zhang and H. Duan, *Small*, 2022, **18**, 2201628.
3. G. Zhang, Y. Zhao, J. Hu, H. Liu, T. Chen, H. Yu and H. Duan, *Journal of Materials Chemistry A*, 2022, **10**, 22182-22193.
4. L. Huang, D. Chen, Y. Ding, S. Feng, Z. L. Wang and M. Liu, *Nano Letters*, 2013, **13**, 3135-3139.
5. F. Liu, L. Zeng, Y. Chen, R. Zhang, R. Yang, J. Pang, L. Ding, H. Liu and W. Zhou, *Nano Energy*, 2019, **61**, 18-26.
6. A. K. Singh and D. Sarkar, *Journal of Materials Chemistry A*, 2017, **5**, 21715-21725.
7. M. Liu, Z. Cong, X. Pu, W. Guo, T. Liu, M. Li, Y. Zhang, W. Hu and Z. L. Wang, *Advanced Functional Materials*, 2019, **29**, 1806298.
8. A. Nanwani, K. A. Deshmukh, P. Sivaraman, D. R. Peshwe, I. Sharma, S. J. Dhoble, H. C. Swart, A. D. Deshmukh and B. K. Gupta, *npj 2D Materials and Applications*, 2019, **3**, 45.
9. X. Liu, W. Zang, C. Guan, L. Zhang, Y. Qian, A. M. Elshahawy, D. Zhao, S. J. Pennycook and J. Wang, *ACS Energy Letters*, 2018, **3**, 2462-2469.
10. B. S. Soram, J. Y. Dai, I. S. Thangjam, N. H. Kim and J. H. Lee, *Journal of Materials Chemistry A*, 2020, **8**, 24040-24052.
11. B. S. Soram, I. S. Thangjam, J. Y. Dai, T. Kshetri, N. H. Kim and J. H. Lee, *Chemical Engineering Journal*, 2020, **395**, 125019.
12. Z. Lu, X. Wu, X. Lei, Y. Li and X. Sun, *Inorganic Chemistry Frontiers*, 2015, **2**, 184-187.
13. J. Liu, C. Guan, C. Zhou, Z. Fan, Q. Ke, G. Zhang, C. Liu and J. Wang, *Advanced Materials*, 2016, **28**, 8732-8739.
14. H. C. Chen, S. Jiang, B. Xu, C. Huang, Y. Hu, Y. Qin, M. He and H. Cao, *Journal of Materials Chemistry A*, 2019, **7**, 6241-6249.
15. H. Zhang, X. Zhang, H. Li, Y. Zhang, Y. Zeng, Y. Tong, P. Zhang and X. Lu, *Green Energy & Environment*, 2018, **3**, 56-62.
16. Y. Fu, X. Cai, H. Wu, Z. Lv, S. Hou, M. Peng, X. Yu and D. Zou, *Advanced Materials*, 2012, **24**, 5713-5718.
17. J. C. Zhuanpei Wanga, Qun Guana, Hui Huanga, Yinchuan Lia, Jingwen Zhoua, Wei Nia,Bin Wanga,Sisi Heb, Huisheng Pengb, *Nano Energy* 2018, **45**.
18. Z. Wang, J. Cheng, Q. Guan, H. Huang, Y. Li, J. Zhou, W. Ni, B. Wang, S. He and H. Peng, *Nano Energy*, 2018, **45**, 210-219.
19. J. Liu, G. Shen, S. Zhao, X. He, C. Zhang, T. Jiang, J. Jiang and B. Chen, *Journal of Materials Chemistry A*, 2019, **7**, 8184-8193.
20. J. Choi, D. Nam, D. Shin, Y. Song, C. H. Kwon, I. Cho, S. W. Lee and J. Cho, *ACS Nano*, 2019, **13**, 12719-12731.
21. G. Sun, H. Yang, G. Zhang, J. Gao, X. Jin, Y. Zhao, L. Jiang and L. Qu, *Energy & Environmental Science*, 2018, **11**, 3367-3374.
22. T. Xin, Y. Wang, N. Wang, Y. Zhao, H. Li, Z. Zhang and J. Liu, *Journal of Materials Chemistry A*, 2019, **7**, 23076-23083.
23. Z. Fan, J. Jin, C. Li, J. Cai, C. Wei, Y. Shao, G. Zou and J. Sun, *ACS Nano*, 2021, **15**, 3098-3107.
24. L. Li, W. Liu, K. Jiang, D. Chen, F. Qu and G. Shen, *Nano-Micro Letters*, 2021, **13**, 100.
25. H. He, H. Tong, X. Song, X. Song and J. Liu, *Journal of Materials Chemistry A*, 2020, **8**, 7836-7846.